Extreme Mechanics Letters 18 (2018) 9–18

Contents lists available at ScienceDirect

Extreme Mechanics Letters

journal homepage: www.elsevier.com/locate/eml

Enhanced out-of-plane compressive strength and energy absorption of 3D printed square and hexagonal honeycombs with variable-thickness cell edges

Shengyu Duan [a,b], Yong Tao [d], Hongshuai Lei [a,b], Weibin Wen [c], Jun Liang [a,b,*], Daining Fang [a,b]

[a] State Key Laboratory of Explosion Science and Technology, Beijing Institute of Technology, Beijing 100081, China
[b] Collaborative Innovation Center of Electric Vehicles in Beijing, Beijing 100081, China
[c] School of Aeronautics and Astronautics, Central South University, Changsha 410083, China
[d] State Key Laboratory of Coal Mine Disaster Dynamics and Control, College of Aerospace Engineering, Chongqing University, Chongqing 400044, China

ARTICLE INFO

Article history:
Received 15 August 2017
Received in revised form 29 September 2017
Accepted 29 September 2017
Available online 24 October 2017

Keywords:
Honeycomb
Out-of-plane compression
Compressive strength
Energy absorption

ABSTRACT

Honeycomb structures have significant advantages in load-bearing and energy absorption. In recent years, some researches have been carried out on the in-plane mechanical properties of honeycombs with variable-thickness cell edges, but the out-of-plane compressive properties of this type of honeycombs have not been well studied. In this paper, the out-of-plane compressive properties of honeycombs with variable-thickness cell edges are investigated through experimental analysis. Here square and hexagonal honeycombs with variable-thickness cells are described with one geometric parameter. The experimental samples of these honeycombs were fabricated using 3D printing technology, and the quasi-static compression tests of these honeycombs were conducted. Experimental results illustrate that the honeycombs with variable-thickness cell edges show enhanced compressive mechanical properties compared to the conventional honeycombs. The highest increase rates of compressive strength of the presented square and hexagonal honeycombs are around 57% and 19%, respectively. In addition, the highest increase rate of specific energy absorption of these square honeycombs reaches up to 172%. The deformation and failure modes of square and hexagonal honeycombs with different geometric parameter values are also discussed and compared. Experimental results show that the square honeycombs with appropriate geometric parameter can achieve more desirable damage tolerance than the conventional square honeycombs.

1. Introduction

In last decades, with the high specific stiffness, strength and high energy absorption ability [1–3], ultra-lightweight cellular materials [3] have been increasingly used as structure material in many fields such as aerospace [4], transportations [5], architecture [6] and biomedicine [7]. Honeycombs, as a typical two-dimensional ultra-lightweight cellular material, have been widely investigated in terms of their excellent mechanical properties and various topological configurations [8–12]. The honeycombs have different mechanical properties along the in-plane and out-of-plane directions. In particular, the out-of-plane stiffness and strength of honeycombs are much higher than their in-plane stiffness and strength due to the different in-plane and out-of-plane deformation mechanisms of honeycombs [3,8]. Actually, a large number of investigations have been conducted through experimental [13–17], numerical [18–21] and analytical [22–24] methods to study the out-of-plane mechanical properties of honeycombs. Some investigations demonstrate that the parent material property [25], topological configuration [26] and relative density [27] of honeycombs have significant influence on the out-of-plane mechanical properties [8,28–30]. Especially, when the relative density of honeycombs is less than 0.05, such as the aluminum foil honeycombs, the honeycombs subject to out-of-plane compression exhibit elastic buckling, which can be clearly observed in the cell level, and then, the cell walls are crushed with progressive folds [13,31]. Comparatively, when the relative density is larger than 0.05, such as the stainless steel square honeycombs, the cell occurs periodic, axial–torsional buckling while the vertical nodal axis remains straight and cell wall segments rotate about the axis [21,28,29].

* Corresponding author at: State Key Laboratory of Explosion Science and Technology, Beijing Institute of Technology, Beijing 100081, China.
E-mail addresses: wenwbin@126.com (W.B. Wen), liangjun@bit.edu.cn (J. Liang).

https://doi.org/10.1016/j.eml.2017.09.016
2352-4316/

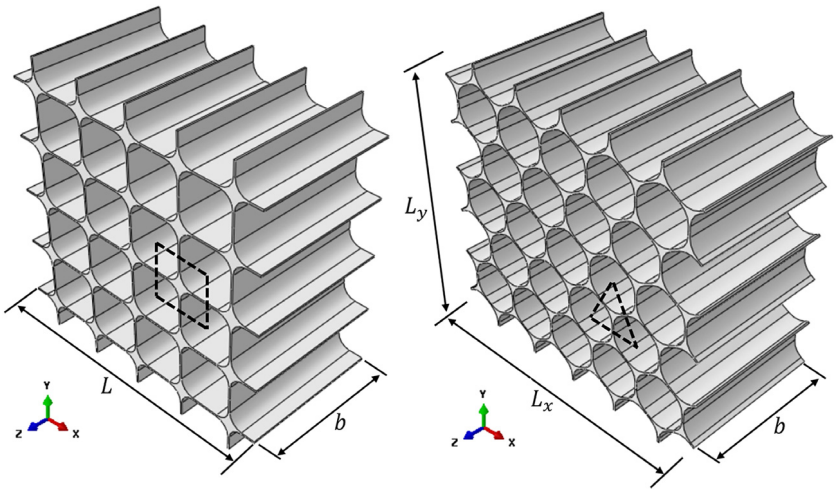

Fig. 1. The structure configuration of square and hexagonal honeycombs with variable-thickness cell edges: the honeycomb width b; the honeycomb length, L (L_x/Ly).

The solid distribution along the honeycomb cell edges plays an important role in determining the in-plane and out-of-plane mechanical properties of honeycombs. The effects of solid distribution on in-plane properties have been investigated by many researchers [32–37]. The results indicate that the solid distribution can significantly influence the elastic and plastic in-plane properties of honeycombs. However, at present, the effects of solid distribution on out-of-plane properties have not been well understood. The earlier researches on the out-of-plane properties of honeycombs with variable-thickness cell edges are focused on the elastic properties such as elastic modulus, shear modulus, compression buckling strength and shear buckling strengths. The relationships between the elastic properties and the geometric parameter of the material distribution of the cell edges are investigated by conducting a series of finite element analysis. High relative density honeycombs with variable-thickness cell edges present higher compressive buckling strength than the conventional honeycombs with constant-thickness cell edges [38]. It is noteworthy that extant researches often study the honeycombs with variable-thickness cell edges by theoretical and finite element methods [20,32,33,35,38]. Because of the complexity of theoretical analysis and finite element analysis, only elastic modulus and yield strength of the material are considered in current researches. However, in practical analysis, the parent material of honeycombs often occur failure under large out-of-plane compression deformation, so experimental observation of the whole crushing process is of great necessity to understand the plastic and failure behavior of the honeycombs. Moreover, extant researches on the effect of solid distribution only focus on the hexagonal honeycombs, and the effect of solid distribution on the square honeycombs need to be clarified.

Recently, many honeycomb-like structures have been fabricated with additive manufacturing due to its excellent flexibility with complex geometric shapes compared with the conventional manufacturing methods [39–43], and honeycombs with variable-thickness cell edges also can be easily fabricated using soft or hard elastic based materials. At present, there are few investigations devoted to the mechanical properties of additively manufactured honeycombs with variable-thickness cell edges. In this paper, the effects of solid distribution in hexagonal and square honeycomb cell edges on the out-of-plane mechanical properties are deliberately investigated. Firstly, square and hexagonal honeycombs with variable-thickness cell edges were fabricated using 3D printer Objet Connex350 with VeroWhitePlus as the base material. Then, the deformation and failure modes of honeycombs with different solid distributions in cell edges are observed and discussed. Finally, their mechanical properties such as the compressive strength and energy absorption are measured by quasi-static out-of-plane compression test. Experimental results illustrate that the proposed additive-manufacturing honeycombs have enhanced out-of-plane mechanical properties compared with the conventional honeycombs.

2. Cell geometry

Two idealized square and hexagonal honeycomb with variable-thickness cell edges on the x-y plane is schematically illustrated in Fig. 1, where b is the honeycomb width along the z direction and L is the honeycomb length. A representative volume element (RVE) model surrounded with dashed lines is also shown in Fig. 1. Geometry configuration of the honeycombs are illustrated in Fig. 2, where t is the thickness outside the intersection of the cell edges, R_p is the radius of the intersection, L_c is the length of the repeating cell element. Relative density is the most important structure characteristics of cellular material, which is dependent on the configuration of the cellular material. It is defined by the ratio of the density of a cellular material ρ^* (i.e., the honeycomb material) to the density of parent material ρ_s [3]. The relative density of the square and hexagonal honeycomb can be geometrically obtained directly from the RVE configuration (see, Fig. 2) as

$$\frac{\rho^*}{\rho_s} = \frac{A_p + A_e}{A_t} = \left(2\frac{R_p}{L_c} + \frac{t}{L_c}\right)^2 - \pi\left(\frac{R_p}{L_c}\right)^2 + 4\frac{t}{L_c}\left(\frac{1}{2} - \frac{R_p}{L_c} - \frac{1}{2}\frac{t}{L_c}\right) \tag{1a}$$

$$\frac{\rho^*}{\rho_s} = \frac{A_p + A_e}{A_t} = \frac{2}{\sqrt{3}}\frac{t}{L_c} - \frac{1}{3}\left(\frac{t}{L_c}\right)^2 + \left(\frac{4}{3} - \frac{2\pi}{3\sqrt{3}}\right)\left(\frac{R_p}{L_c}\right)^2 \tag{1b}$$

where $A_p = \left(t + 2R_p\right)^2 - \pi R_p^2$ for square honeycomb and $A_p = \left(2R_p + t\right)^2\sqrt{3}/4 - R_p^2\pi/2$ for hexagonal honeycomb are the areas of the material within the intersection at the vertex, $A_e = 4L_c(L_c - t - 2R_p)$ for square honeycomb and $A_e = 3t(L_c/2 - R_p/\sqrt{3} - t/2\sqrt{3})$ for hexagonal honeycomb are the area of the material in the cell edges outside the intersection. $A_t = L_c^2$ for square honeycomb and $A_t = 3\sqrt{3}L_c^2/4$ for hexagonal honeycomb are the areas of the RVE. It is noteworthy that the relative density of the honeycombs ρ^*/ρ_s in Eq. (1) can be determined by the ratios R_p/L_c and t/L_c.

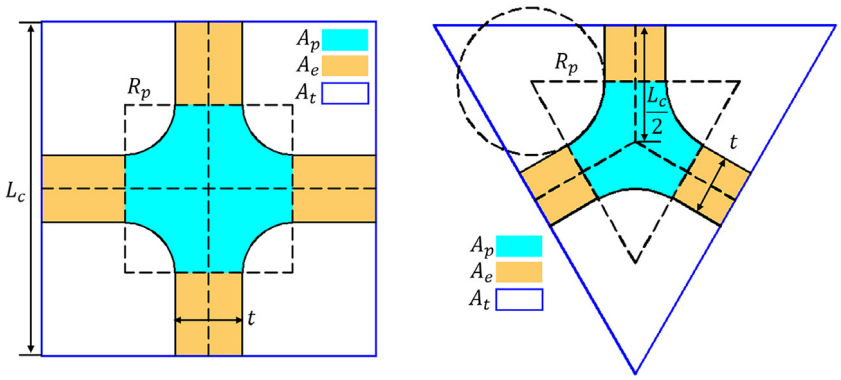

Fig. 2. The representative volume element (RVE) model of square and hexagonal honeycombs with variable-thickness cell edges: the thickness outside the intersection of the cell edges t; the radius of the intersection R_p; the length of the repeating cell element L_c; the area within the intersection at the vertex A_p; the area in the cell edges outside the intersection A_e; the areas of the RVE A_t.

Here we adopted a geometric parameter Φ_2 introduced by Simone and Gibson [35] to describe the proportion of the variable-thickness cell edges, and the geometric parameter Φ_2 is defined as the area ratio of the intersection region A_p to the total solid region $A_p + A_e$ in the RVE model, and given by:

$$\Phi_2 = \frac{A_p}{A_p + A_e} = \frac{\rho_s}{\rho^*}\left[(4-\pi)\left(\frac{R_p}{L_c}\right)^2 + 4\left(\frac{R_p}{L_c}\right)\left(\frac{t}{L_c}\right) + \left(\frac{t}{L_c}\right)^2\right] \tag{2a}$$

for square honeycomb and

$$\Phi_2 = \frac{A_p}{A_p + A_e} = \frac{\rho_s}{\rho^*}\left[\left(\frac{4}{3} - \frac{2\pi}{3\sqrt{3}}\right)\left(\frac{R_p}{L_c}\right)^2 + \frac{4}{3}\left(\frac{R_p}{L_c}\right)\left(\frac{t}{L_c}\right) + \frac{1}{3}\left(\frac{t}{L_c}\right)^2\right] \tag{2b}$$

for hexagonal honeycomb.

In following analysis, the relative density ρ^*/ρ_s in Eq. (2) is kept as constant, and several representative values of R_p/L_c and t/L_c are chosen to obtain different values of geometric parameter Φ_2.

3. Sample design and preparation

To investigate the influence of the geometric parameter Φ_2 on the out-of-plane mechanical properties of square and hexagonal honeycombs, four Φ_2 values are selected for both the square and hexagonal honeycombs. The detailed dimensions and geometric parameter values of each honeycomb are listed in Table 1. The definitions of each geometric parameter in Table 1 can be found in Figs. 1 and 2. Three specimens of each configuration were fabricated using an Object 350 Connex3 3D printer (Stratasys Ltd., USA) with the built material VeroWhitePlus. This material, offered by Stratasys, is of desirable stiffness and strength, and is appropriate for this study. The specimens were fabricated along the z-direction (i.e., the build direction as shown Fig. 1) to avoid the supporting material filled in the void of the honeycombs. The manufactured samples are displayed in Fig. 3(a) where all samples are in good quality. Table 2 lists the designed mass and measured mass of all experiment samples. Three samples of each configuration were fabricated for test. In order to determine the mechanical properties of the parent material VeroWhitePlus, uniaxial tensile samples are prepared with the same manufacturing method and circumstances as the honeycomb samples. Typical tension specimens and their geometric dimensions are depicted in Fig. 3(b). Three as-fabricated tensile samples are illustrated in Fig. 3(c). The uniaxial tensile tests were performed on a 30 kN Instron testing machine at a displacement rate of 1 mm/min. The out-of-plane compression tests were carried out on a 300 KN universal testing machine with the crosshead speed of 1 mm/min. Force–displacement data were recorded to calculate the stress–strain curves of the samples.

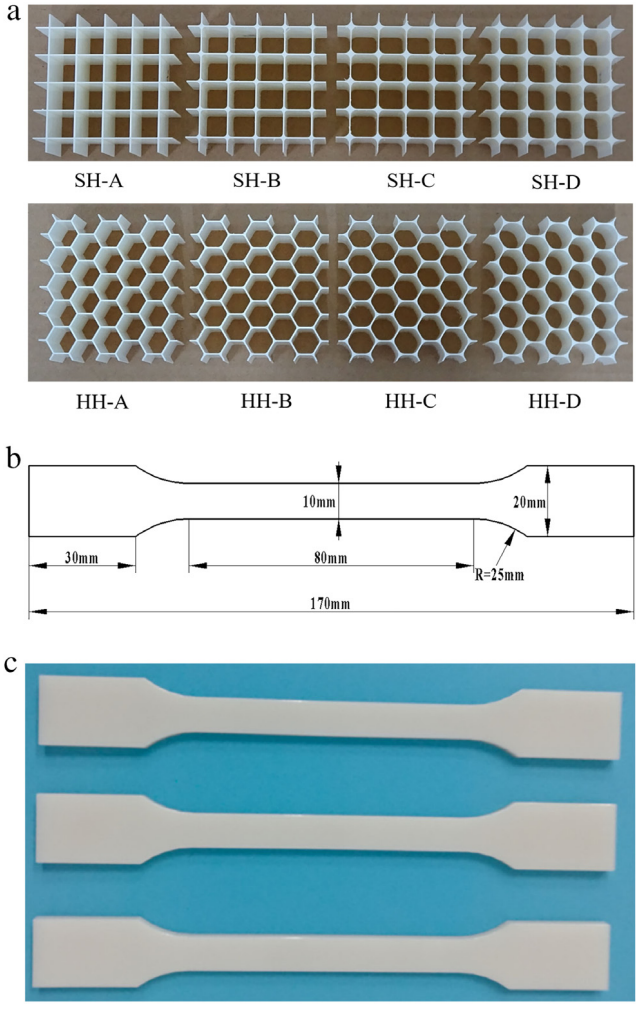

Fig. 3. (a) 3D printed square and hexagonal honeycomb samples; (b) Geometric dimensions of dog–bone shaped samples; (c) 3D printed dog–bone shaped samples for experimental tests.

Table 1
Geometric parameters of honeycomb unit cells.

Sample	ρ^*/ρ_s	L_x/L_y (mm)	b (mm)	L_c (mm)	Φ_2 (%)	t (mm)	R_p (mm)
SH-A	0.11	80	40	16	2.89	0.9	0
SH-B					34.59	0.8	1.88
SH-C					61.97	0.6	3.26
SH-D					79.58	0.4	4.23
HH-A	0.11	80.97/76.5	40	8.5	2.89	0.83	0
HH-B					33.15	0.78	1.89
HH-C					61.23	0.66	3.55
HH-D					79.98	0.52	4.82

Table 2
Difference between design mass and measured mass.

Sample	Designed mass (g)	Measured mass (g)
SH-A	33.20	34.05
SH-B		34.90
SH-C		35.57
SH-D		36.12
HH-A	32.20	34.15
HH-B		34.19
HH-C		35.13
HH-D		36.18

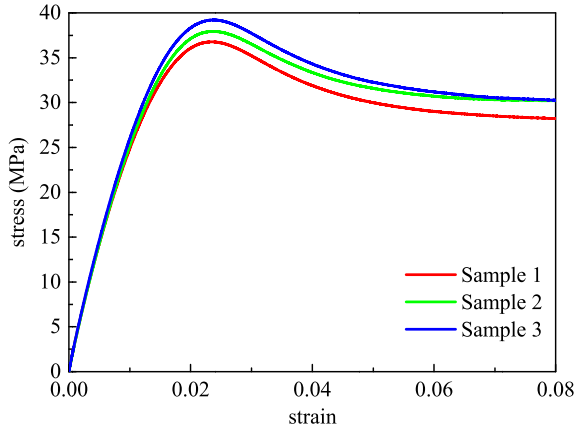

Fig. 4. The stress–strain curves of dog–bone shaped samples under uniaxial tension.

4. Results and discussion

4.1. Parent material mechanical properties

The typical stress–strain curves for the three uniaxial tensile samples are shown in Fig. 4. The elastic modulus and tensile strength obtained from the stress–strain curves are listed in Table 3. The Poisson's ratio in Table 3 is obtained from Ref. [44]. It can be found that the acrylic polymer material VeroWhitePlus shows low strain hardening effect, which is different from the metal materials such as stainless steel.

4.2. Deformation and failure modes

In this study, all stress–strain curves were obtained from the force–displacement data recorded in the compression tests. All compression stress–strain curves for the design models are illustrated in Fig. 5, where the curves show acceptable repeatability. For the square honeycombs, the stress–strain curves in Fig. 5(a) describe the whole out-of-plane compression process which can be divided into five phases as: (i) elastic deformation; (ii) elastic buckling; (iii) plastic yielding; (iv) initial brittle fracture; (v) final brittle fracture. Fig. 6(a) displays the detailed deformation and failure modes of these phases. As for the hexagonal honeycombs, the compression behavior is quite different from that of the square honeycombs. The stress–strain curves in Fig. 5(b) are similar to those of the metal hexagonal honeycombs under out-of-plane compression [21,28]. As shown in Fig. 5(b), the stress–strain curves have an initial linear elastic region followed by a plateau stress region and finally a rapidly increasing densification region [3]. But the compression behavior of 3D printed hexagonal honeycomb is quite different from the metal hexagonal honeycombs. The detailed deformation and failure modes of hexagonal honeycombs are illustrated in Fig. 6(b).

As shown in Fig. 6(a), the deformation and failure modes of square honeycombs with variable-thickness cell edges vary with the increase of geometric parameter Φ_2. Firstly, the elastic phase shows consistency of the four different parameters. Then, when the honeycombs turned into elastic buckling phase, the buckling half wavelength reduced with the increasing of Φ_2, which means the increasing of compressive buckling strength. Next, the honeycombs passed into plastic buckling phase. In this phase, the stress–strain curves present a plateau with lower stress values.

Moreover, the duration of this phase depends on the geometric parameter Φ_2 of the honeycombs, the brittle fractures occurred in the honeycomb cells. For square honeycombs with small Φ_2, such as SH-A and SH-B, the initial cracks on the honeycomb cells were in a hole shape, while for square honeycombs with large Φ_2, such as SH-C and SH-D, the initial cracks were in a linear shape along the compression direction. This is because square honeycombs with larger Φ_2 have thicker cell walls at the intersection region. Finally, more cracks occurred and extended rapidly, leading to final brittle failure. For square honeycombs with small Φ_2, the final failure was perpendicular to the compression direction, and for square honeycombs with large Φ_2, the final failure was along the compression direction. Thus, it can be seen that appropriate variable-thickness cell edges can effectively extend the compressive strain of the square honeycombs. The detail mechanical properties of square honeycombs influenced by the variable-thickness cell edges will be discussed in Section 4.3.

Fig. 6(b) shows the compression configurations of hexagonal honeycombs with different geometric parameters Φ_2. The initial elastic deformation modes of the four models are similar. Then, the honeycombs turned into elastic and plastic buckling phase. It is noteworthy that at the first fold of the honeycombs (strain 0.08–0.18), the honeycombs with large Φ_2 provide large compressive stress, which can be seen in Fig. 5(c). As the compression strain

Table 3
Material properties of VeroWhitePlus.

Material	Density (g/cm^3)	Young's modulus (GPa)	Tensile strength (MPa)	Poisson's ratio
VeroWhitePlus	1.18	2.18	37.98	0.33 [36]

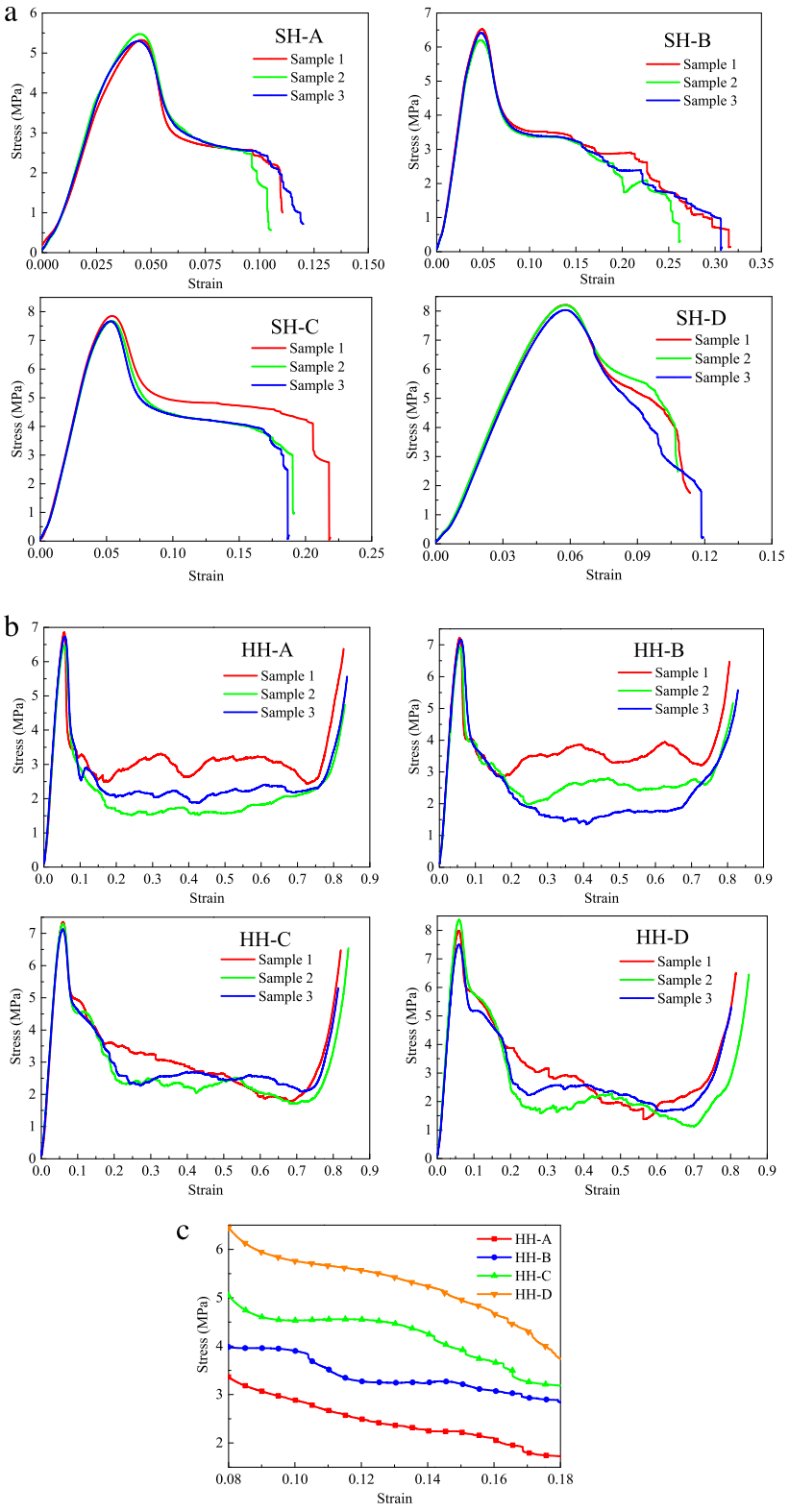

Fig. 5. The stress–strain curves of (a) square and (b) hexagonal honeycomb samples. (c) The stress–strain curves of different hexagonal honeycombs samples at strain 0.08–0.18.

increases, the honeycombs cells continue to fold and produce initial cracks. Meanwhile, the stress–strain curves turned into plateau region. Unlike square honeycombs, the initial crack of hexagonal honeycombs could not extend easily to cause final brittle fracture failure. In a long compressive phase, the initial cracks extended along the honeycomb cells slowly and created a stable plateau on the stress–strain curves. Finally, the honeycombs turned into densification phase and the stress–strain curve increased steeply.

It can be seen that the geometric parameter Φ_2 illustrates little influence on the compressive deformation and failure configuration of the hexagonal honeycombs, and the detailed mechanical

Table 4
The mechanical properties and SEA of the square and hexagonal honeycomb samples.

Sample	Strength (MPa)	Elastic modulus (MPa)	Maximal compressive strain	SEA (kJ/kg)
SH-A	5.37	177.58	0.1119	0.33
SH-B	6.38	189.12	0.2955	0.87
SH-C	7.73	196.88	0.1992	0.90
SH-D	8.15	188.69	0.1136	0.56
HH-A	6.68	158.26	–	15.66
HH-B	7.10	165.97	–	18.13
HH-C	7.25	168.19	–	17.98
HH-D	7.95	181.85	–	17.97

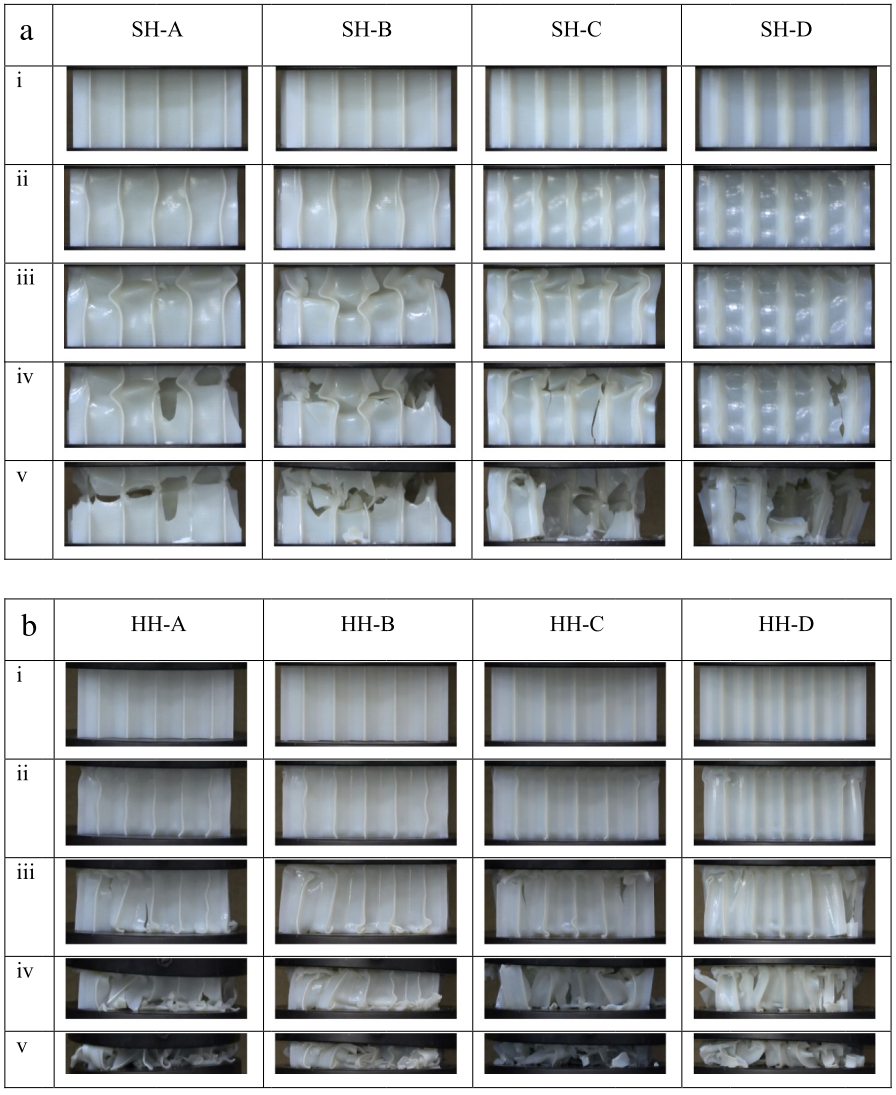

Fig. 6. (a) Sequence of deformed configurations of square honeycombs with different geometric parameters: (i) elastic deformation; (ii) elastic buckling; (iii) plastic yielding; (iv) initial brittle fracture; (v) final brittle fracture. (b) Sequence of deformed configurations of hexagonal honeycombs with different geometric parameters: (i) elastic deformation; (ii) plastic yielding; (iii) initial brittle fracture; (iv) subsequent brittle fracture; (v) final brittle fracture.

properties influenced by the variable-thickness cell edges will be discussed in Section 4.3.

4.3. Mechanical properties and energy absorption

As illustrated in Figs. 1 and 2, the geometric parameter Φ_2 defines the solid distribution of the square and hexagonal honeycomb cells. As the parameter Φ_2 increases, the mass around the intersection region increases correspondingly. Table 4 lists all mechanical properties and energy absorption characteristics of the presented honeycombs that are compared in following analysis. In Fig. 7, the elastic modulus of the presented honeycombs displays small fluctuation for different Φ_2 values due to inevitable manufacturing inaccuracy, which is also demonstrated by Table 2, but is roughly consistent with the predicted modulus that is a function in terms of the relative density of the honeycomb [3].

In Fig. 8, the compressive strength results of the square and hexagonal honeycombs with different geometric parameter Φ_2 values are presented. Here the compressive strength is actually the initial peak stress of the stress–strain curves in Fig. 5. It can be observed in Fig. 8 that the compressive strength increases monotonously as the geometric parameter Φ_2 value increases. For

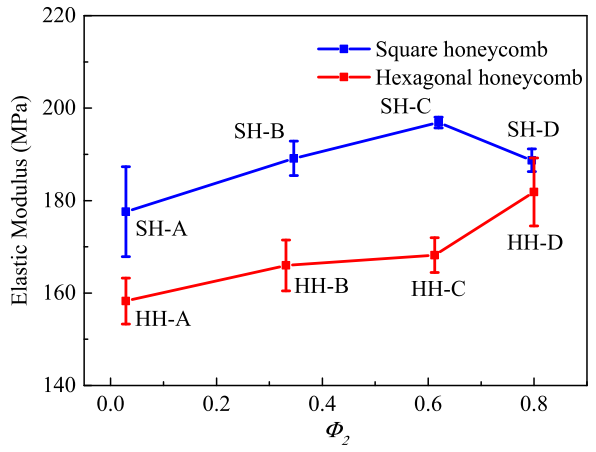

Fig. 7. The elastic modulus of square and hexagonal honeycombs with different geometric parameters.

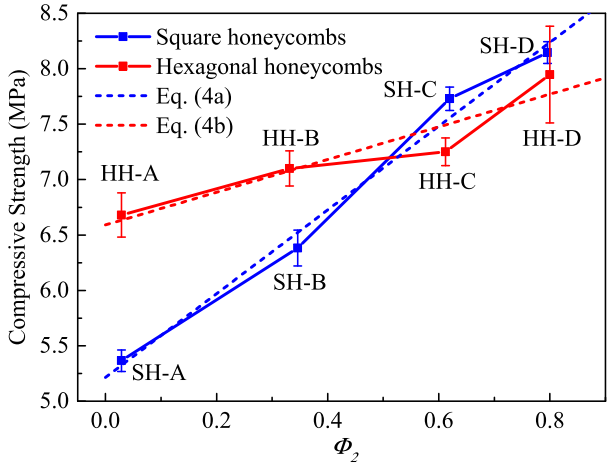

Fig. 8. The compressive strength of square and hexagonal honeycombs with different geometric parameters.

square honeycombs, the compressive strength of the conventional configuration (SH-A) is about 5.37 MPa. When the geometric parameter Φ_2 value is 79.58%, the compressive strength of square honeycombs (SH-D) with variable-thickness cell edges is up to ∼8.15 MPa that increases by ∼52% when compared with the compressive strength of the SH-A. As for hexagonal honeycombs, the compressive strength of the conventional configuration (HH-A) is ∼6.68 MPa, which is higher than that of the corresponding conventional square honeycomb configuration (SH-A). When the geometric parameter Φ_2 is 79.98%, the hexagonal honeycombs with variable-thickness cell edges (HH-D) have about 7.95 MPa compressive strength that is about 19% increase in strength when compared with the HH-A configuration. The curves in Fig. 8 illustrate, for different geometric parameter Φ_2 values, the presented square honeycombs show more obvious improvement in compressive strength than the hexagonal ones when compared with the corresponding conventional ones.

Moreover, it is worth noting that the compressive strength of the square and hexagonal honeycombs with variable-thickness cell edges is approximately increased with the increase of geometric parameter Φ_2. From the discussion of the deformation modes in the previous section, it can be found that the out-of-plane compressive strength is mainly dependent on the elastic buckling of the cell edges, and an estimation formula is proposed here to express the effects of Φ_2 on compressive strength. For the square and hexagonal honeycombs with constant-thickness cell edges, the out-of-plane compressive buckling strength can be, respectively, expressed as [3]

$$\frac{\sigma_{SH}}{E_s} = \frac{K_{SH}}{4\left(1-\nu_s^2\right)}\left(\frac{\rho^*}{\rho_s}\right)^3 \tag{3a}$$

for square honeycombs and

$$\frac{\sigma_{HH}}{E_s} = \frac{3K_{HH}}{4\left(1-\nu_s^2\right)}\left(\frac{\rho^*}{\rho_s}\right)^3 \tag{3b}$$

for hexagonal honeycombs. Here, K_{SH} and K_{HH} are end constraint factors, depending upon the ratio b/L_c as well as the boundary conditions at top and bottom edges. The end constraint factor can be determined theoretically, numerically or experimentally. Here, K_{SH} and K_{HH} are obtained as 6.70 and 2.78, respectively, from the compression test results of sample SH-A and HH-A. Then, the out-of-plane compressive buckling strength of honeycombs with variable-thickness can be, respectively, expressed as:

$$\frac{\sigma_{SH}\left(\Phi_2\right)}{E_s} = \frac{K_{SH}}{4\left(1-\nu_s^2\right)}\left(\frac{\rho^*}{\rho_s}\right)^3\left(k_{SH}\Phi_2+1\right) \tag{4a}$$

for square honeycombs and

$$\frac{\sigma_{HH}\left(\Phi_2\right)}{E_s} = \frac{3K_{HH}}{4\left(1-\nu_s^2\right)}\left(\frac{\rho^*}{\rho_s}\right)^3\left(k_{HH}\Phi_2+1\right) \tag{4b}$$

for hexagonal honeycombs, where $k_{SH} = 0.704$ and $k_{HH} = 0.221$ are the fitting parameters, which are obtained from a linear fitting. The results from Eqs. (4a) and (4b) are compared with the experimental results, as plotted in Fig. 8. It can be seen that introducing the variable-thickness cell edges can improve the compressive strength of square and hexagonal honeycombs greatly.

Energy absorption capacity is one of the key indicators in characterizing honeycomb materials for impact resistance and energy absorption applications. The energy absorption capacity can be calculated by the area under the nominal stress–strain curve. The energy absorbed per unit volume is defined as [3]

$$U_V = \int_0^{\varepsilon} \sigma\, d\varepsilon \tag{5a}$$

Along with the energy absorbed per unit volume, the specific energy absorption (SEA), namely absorbed energy per unit mass, is also an important indicator. As mass is critical for energy absorbers in practical applications, the SEA of honeycombs is defined as [24,45]:

$$U_M = \frac{U_V}{\rho^*} \tag{5b}$$

where ρ^* is the density of honeycombs. In general, higher SEA values means better energy absorbing capacity of cellular materials. Here, SEA is adopted to evaluate the energy absorbing capacity of honeycombs with variable-thickness cell edges under out-of-plane compression.

In Fig. 9(a), the SEA variation of the square honeycombs with variable-thickness edges are plotted versus the geometric parameter Φ_2. It can be observed that, the SEAs of all square honeycombs with variable-thickness edges are clearly higher than that of the referred conventional square honeycomb. Notably, the SH-B and SH-C samples show almost 172% increase in SEA than the conventional SH-A samples. Further, Fig. 9(b) illustrates the maximal compressive strain and the mean crushing stress of all square honeycomb samples, which are two factors determining the actual SEA. The quantified effect of geometric parameter Φ_2 on maximal compressive strain and the mean crushing stress of all samples is shown in Fig. 9(b). It shows that high SEA can be

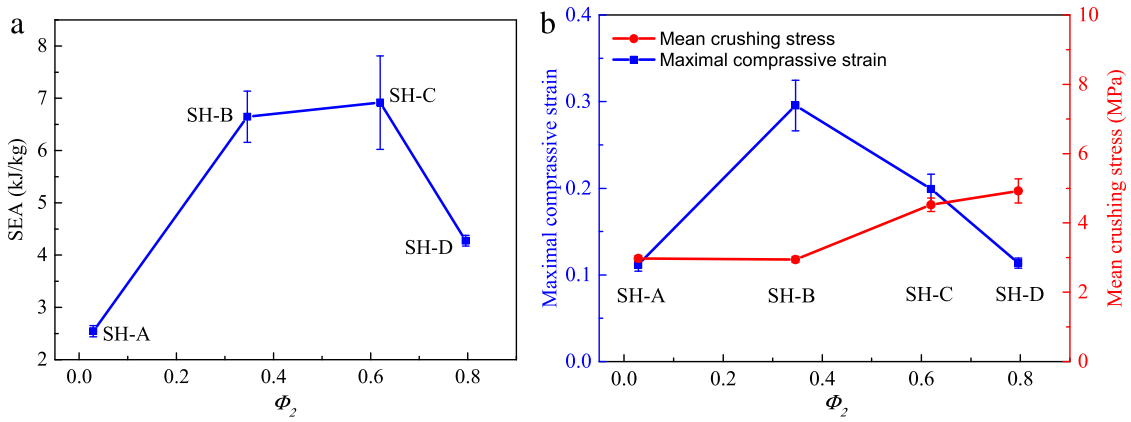

Fig. 9. (a) SEA and (b) maximal compressive strain and mean crushing stress of square honeycombs with different geometric parameters.

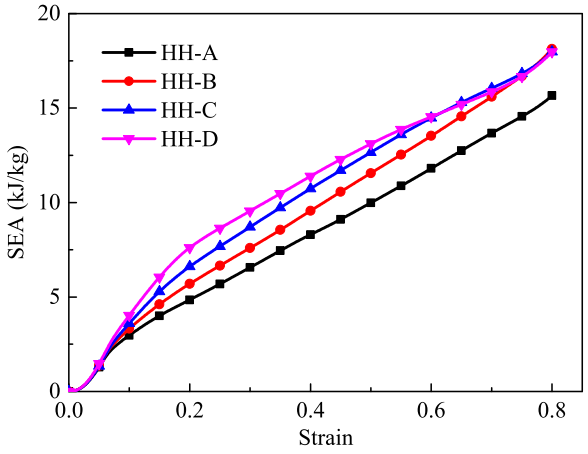

Fig. 10. The SEA of hexagonal honeycombs with different geometric parameters during the compression process.

obtained when appropriate parameter Φ_2 is selected. It can be noticed that, as the parameter Φ_2 increases, the mean crushing stress also increases. In the figure, when $\Phi_2 = 34.59$, the SH-B samples show small increase in the mean crushing stress, but large increase in the maximal compressive strain, and thus, lead to high SEA; as for $\Phi_2 = 61.97$, both of the mean crushing stress and the maximal compressive strain of the SH-C samples have considerable improvement, which results in highest SEA among all SH samples. In conclusion, high SEA can be obtained for the square honeycombs with variable-thickness cell edges when appropriate geometric parameter Φ_2 is selected.

As for the hexagonal honeycombs, the SEA curves of all samples within the compression process are plotted in Fig. 10 where all proposed HH samples give higher SEA than the conventional HH samples. For relatively small compression strain, the SEAs of the proposed HH samples increase with the increase of parameter Φ_2. But, for large compression strain, the SEA curves of all proposed HH samples (HH-B, HH-C and HH-D) gradually approach to each other, however, still higher than that of the conventional samples (HH-A).

4.4. Comparison with competing topologies

The performance of 3D printed honeycombs in this study is compared with that of competing topologies. In terms of the lack of the experiment data for the 3D printed honeycombs and lattice structures, several categories of competing topologies made by conventional metals are selected to compare with the 3D printed honeycombs in this study. Fig. 11(a) compare the compressive strength of the honeycombs in this study with competing topologies, including 304 stainless steel (SS) square honeycombs [29], 304 stainless steel hollow pyramidal lattice truss structures [46], 304 stainless steel corrugations [47], Al honeycomb-corrugation hybrid sandwich core (HBC) [48], Ti-6Al-4V pyramidal [49], 304 stainless steel pyramidal [50] and 304 stainless steel single and double corrugations [51]. In the figure, when the compressive strength between 5 and 10 MPa, the 3D printed honeycombs with variable-thickness cell edges exhibit smaller density than most of the competing topologies. Fig. 11(b) compares the specific energy absorption of the proposed honeycombs with competing topologies, including Al lattice truss [52], hollow lattice truss [53], hollow pyramidal truss [54] and steel square honeycombs [55]. It can be noticed that the SEA of hexagonal honeycombs are similar to the Al lattice truss, and larger than the SEA of most of the competing topologies.

5. Conclusions

In this study, the out-of-plane compressive properties of square and hexagonal honeycombs with variable-thickness cell edges fabricated by additive manufacturing were investigated. The square and hexagonal honeycombs were designed with geometric parameters Φ_2, and the corresponding experiment samples are manufactured using PolyJet 3D printing technology with the built material VeroWhitePlus. It is noteworthy that 3D printing technology is a superior choice for the proposed honeycombs when compared with the conventional manufacturing methods such as slotted assembly approach and expansion manufacturing process. All experiment samples are of the same relative density. The out-of-plane compressive experiment shows good repeatability. With appropriate geometric parameter Φ_2, the proposed honeycombs value can obtain excellent out-of-plane compressive mechanical properties.

For the deformation and failure modes of the honeycombs with variable-thickness cell edges, the proposed square honeycombs show enhanced damage tolerance than the conventional square honeycombs. When $\Phi_2 = 34.59\%$, the maximal compressive strain of square honeycombs is 200% higher than the conventional square honeycombs. It is worth noting that the acrylic polymer material VeroWhitePlus used in this study shows low strain hardening effect.

For square honeycombs, samples with geometric parameter $\Phi_2 = 79.58\%$ has 52% higher compressive strength than the conventional square honeycombs, while samples with $\Phi_2 = 61.97\%$ has 172% higher specific energy absorption than the conventional

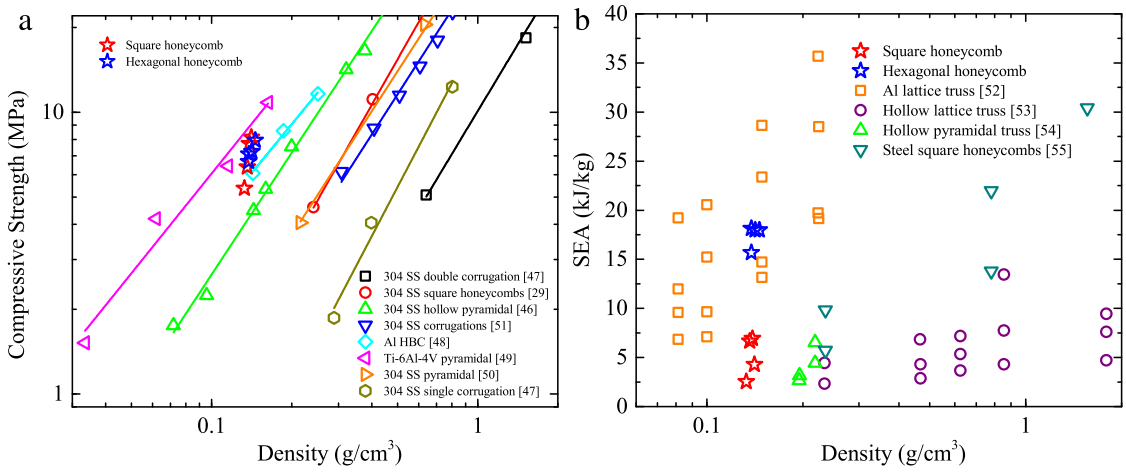

Fig. 11. (a) Compressive strength and (b) SEA of light-weight honeycomb/lattice core materials.

square honeycombs. As for the hexagonal honeycombs, samples with $\Phi_2 = 79.98\%$ has 19% higher compressive strength than the conventional hexagonal honeycombs, while samples with $\Phi_2 = 33.15\%$, 61.97% and 79.98% have higher specific energy absorption than the conventional hexagonal honeycombs. In addition, the specific energy absorption (SEA) of hexagonal honeycombs increases with the geometric parameter Φ_2 for relatively small compression strain.

From the above, it can be seen that the proposed honeycombs with variable-thickness cell edges show enhanced out-of-plane compressive strength and energy absorption ability when compared with conventional honeycombs with constant-thickness cell edges. Geometric parameter Φ_2 depicts the material distribution in the cell edges. Honeycombs with larger geometric parameter Φ_2 present higher compressive strength. Square honeycombs with medium geometric parameter Φ_2 shows excellent damage tolerance and highest energy absorption ability among all geometric parameter values, and hexagonal honeycombs with larger geometric parameter Φ_2 show higher energy absorption ability. In this study, the proposed design concept of honeycomb cells improve the mechanical performance of conventional honeycombs, when using 3D printing technology, and is attractive for practical applications.

Acknowledgments

This research is substantially supported by the National Natural Science Foundation of China (No. 11602004 and No. 11325210) and the Project of Beijing Municipal Science & Technology Commission (Z161100001416007) and the Project of State Key Laboratory of Explosion Science and Technology (ZDKT17–02 and YBKT17–01).

References

[1] N. Wicks, J.W. Hutchinson, Optimal truss plates, Int. J. Solids Struct. 38 (30–31) (2001) 5165–5183.
[2] N. Wicks, J.W. Hutchinson, Performance of sandwich plates with truss cores, Mech. Mater. 36 (8) (2004) 739–751.
[3] L.J. Gibson, M.F. Ashby, Cellular Solids: Structure and Properties, 1997.
[4] P.S. Carlin, I. Ieee, Lightweight mirror systems for spacecraft - An overview of materials & manufacturing needs, in: 2000 Ieee Aerospace Conference Proceedings, Vol. 42000, pp. 169-181.
[5] J. Ju, B. Ananthasayanam, J.D. Summers, P. Joseph, Design of cellular shear bands of a non-pneumatic tire -investigation of contact pressure, SAE Int. J. Passeng. Cars –Mech. Syst. 3 (1) (2010) 598–606.
[6] N.D. Kaushika, P.K. Sharma, R.P. Priya, Solar thermal-analysis of honeycomb roof cover system for energy-conservation in an air-conditioned building, Energy Build. 18 (1) (1992) 45–49.
[7] M. Tanaka, Design of novel 2D and 3D biointerfaces using self-organization to control cell behavior, Biochim. Biophys. Acta 1810 (3) (2011) 251–258.
[8] Q. Zhang, X. Yang, P. Li, G. Huang, S. Feng, C. Shen, B. Han, X. Zhang, F. Jin, F. Xu, T.J. Lu, Bioinspired engineering of honeycomb structure –Using nature to inspire human innovation, Prog. Mater. Sci. 74 (2015) 332–400.
[9] A.J. Wang, D.L. McDowell, In-plane stiffness and yield strength of periodic metal honeycombs, J. Eng. Mater. Technol. 126 (2) (2004) 137.
[10] M.G. Rashed, M. Ashraf, R.A.W. Mines, P.J. Hazell, Metallic microlattice materials: A current state of the art on manufacturing, mechanical properties and applications, Mater. Des. 95 (2016) 518–533.
[11] N.A. Fleck, V.S. Deshpande, M.F. Ashby, Micro-architectured materials: Past, present and future, Proc. R. Soc. A 466 (2121) (2010) 2495–2516.
[12] H.N. Wadley, Multifunctional periodic cellular metals, Phil. Trans. R. Soc. A 364 (1838) (2006) 31–68.
[13] A. Alavi Nia, M.Z. Sadeghi, An experimental investigation on the effect of strain rate on the behaviour of bare and foam-filled aluminium honeycombs, Mater. Des. 52 (2013) 748–756.
[14] I. Elnasri, S. Pattofatto, H. Zhao, H. Tsitsiris, F. Hild, Y. Girard, Shock enhancement of cellular structures under impact loading: Part I Experiments, J. Mech. Phys. Solids 55 (12) (2007) 2652–2671.
[15] Y. Tao, M. Chen, H. Chen, Y. Pei, D. Fang, Strain rate effect on the out-of-plane dynamic compressive behavior of metallic honeycombs: Experiment and theory, Compos. Struct. 132 (2015) 644–651.
[16] S. Xu, J.H. Beynon, D. Ruan, G. Lu, Experimental study of the out-of-plane dynamic compression of hexagonal honeycombs, Compos. Struct. 94 (8) (2012) 2326–2336.
[17] H. Zhao, G. Gary, Crushing behaviour of aluminium honeycombs under impact loading, Int. J. Impact Eng. 21 (10) (1998) 827–836.
[18] L. Aktay, A.F. Johnson, B.H. Kröplin, Numerical modelling of honeycomb core crush behaviour, Eng. Fract. Mech. 75 (9) (2008) 2616–2630.
[19] M. Giglio, A. Manes, A. Gilioli, Investigations on sandwich core properties through an experimental- numerical approach, Composites B 43 (2) (2012) 361–374.
[20] L. Liu, P. Meng, H. Wang, Z. Guan, The flatwise compressive properties of nomex honeycomb core with debonding imperfections in the double cell wall, Composites B 76 (2015) 122–132.
[21] A. Wilbert, W.Y. Jang, S. Kyriakides, J.F. Floccari, Buckling and progressive crushing of laterally loaded honeycomb, Int. J. Solids Struct. 48 (5) (2011) 803–816.
[22] L.L. Hu, T.X. Yu, Dynamic crushing strength of hexagonal honeycombs, Int. J. Impact Eng. 37 (5) (2010) 467–474.
[23] Q.M. Li, H. Meng, Attenuation or enhancement - A one-dimensional analysis on shock transmission in the solid phase of a cellular material, Int. J. Impact Eng. 27 (10) (2002) 1049–1065.
[24] Y. Tao, M. Chen, Y. Pei, D. Fang, Strain rate effect on mechanical behavior of metallic honeycombs under out-of-plane dynamic compression, Trans. ASME, J. Appl. Mech. 82 (2) (2015).
[25] H.X. Zhu, N.J. Mills, The in-plane non-linear compression of regular honeycombs, Int. J. Solids Struct. 37 (13) (2000) 1931–1949.
[26] A.J. Wang, D.L. McDowell, In-plane stiffness and yield strength of periodic metal honeycombs, Trans. ASME, J. Eng. Mater. Technol. 126 (2) (2004) 137–156.
[27] A.J. Wang, D.L. McDowell, Yield surfaces of various periodic metal honeycombs at intermediate relative density, Int. J. Plast. 21 (2) (2005) 285–320.
[28] J. Zhang, M.F. Ashby, The out-of-plane properties of honeycombs, Int. J. Mech. Sci. 34 (6) (1992) 475–489.

[29] F. Côté, V.S. Deshpande, N.A. Fleck, A.G. Evans, The out-of-plane compressive behavior of metallic honeycombs, Mater. Sci. Eng. A 380 (1) (2004) 272–280.
[30] Y. Tao, S. Duan, W. Wen, Y. Pei, D. Fang, Enhanced out-of-plane crushing strength and energy absorption of in-plane graded honeycombs, Composites B 118 (2017) 33–40.
[31] A. Alavi Nia, M.Z. Sadeghi, The effects of foam filling on compressive response of hexagonal cell aluminum honeycombs under axial loading-experimental study, Mater. Des. 31 (3) (2010) 1216–1230.
[32] C.H. Chuang, J.S. Huang, Effects of solid distribution on the elastic buckling of honeycombs, Int. J. Mech. Sci. 44 (7) (2002) 1429–1443.
[33] C.H. Chuang, J.S. Huang, Elastic moduli and plastic collapse strength of hexagonal honeycombs with plateau borders, Int. J. Mech. Sci. 44 (9) (2002) 1827–1844.
[34] J.L. Grenestedt, On interactions between imperfections in cellular solids, J. Mater. Sci. 40 (22) (2005) 5853–5857.
[35] A.E. Simone, L.J. Gibson, Effects of solid distribution on the stiffness and strength of metallic foams, Acta Mater. 46 (6) (1998) 2139–2150.
[36] M.Y. Yang, J.S. Huang, Numerical analysis of the stiffness and strength of regular hexagonal honeycombs with plateau borders, Compos. Struct. 64 (1) (2004) 107–114.
[37] M.Y. Yang, J.S. Huang, J.W. Hu, Elastic buckling of hexagonal honeycombs with dual imperfections, Compos. Struct. 82 (3) (2008) 326–335.
[38] T.C. Lin, M.Y. Yang, J.S. Huang, Effects of solid distribution on the out-of-plane elastic properties of hexagonal honeycombs, Compos. Struct. 100 (2013) 436–442.
[39] S. Babaee, J. Shim, J.C. Weaver, E.R. Chen, N. Patel, K. Bertoldi, 3D soft metamaterials with negative Poisson's ratio, Adv. Mater. 25 (36) (2013) 5044–5049.
[40] A. Ghaedizadeh, J. Shen, X. Ren, Y.M. Xie, Tuning the performance of metallic auxetic metamaterials by using buckling and plasticity, Materials 9 (1) (2016).
[41] J. Shen, S. Zhou, X. Huang, Y.M. Xie, Simple cubic three-dimensional auxetic metamaterials, Phys. Status Solidi b 251 (8) (2014) 1515–1522.
[42] A. Ingrole, A. Hao, R. Liang, Design and modeling of auxetic and hybrid honeycomb structures for in-plane property enhancement, Mater. Des. 117 (2017) 72–83.
[43] S.R.G. Bates, I.R. Farrow, R.S. Trask, 3D printed polyurethane honeycombs for repeated tailored energy absorption, Mater. Des. 112 (2016) 172–183.
[44] P. Zhang, M.A. Heyne, A.C. To, Biomimetic staggered composites with highly enhanced energy dissipation: Modeling, 3D printing, and testing, J. Mech. Phys. Solids 83 (2015) 285–300.
[45] H.S. Kim, New extruded multi-cell aluminum profile for maximum crash energy absorption and weight efficiency, Thin-Walled Struct. 40 (4) (2002) 311–327.
[46] D.T. Queheillalt, H.N.G. Wadley, Hollow pyramidal lattice truss structures, Int. J. Mater. Res. 102 (4) (2011) 389–400.
[47] B. Han, L.L. Yan, B. Yu, Q.C. Zhang, C.Q. Chen, T.J. Lu, Collapse mechanisms of metallic sandwich structures with aluminum foam-filled corrugated cores, J. Mech. Mater. Struct. 9 (4) (2014) 397–425.
[48] B. Han, K. Qin, B. Yu, B. Wang, Q. Zhang, T.J. Lu, Honeycomb–corrugation hybrid as a novel sandwich core for significantly enhanced compressive performance, Mater. Des. 93 (2016) 271–282.
[49] D.T. Queheillalt, H.N.G. Wadley, Titanium alloy lattice truss structures, Mater. Des. 30 (6) (2009) 1966–1975.
[50] F.W. Zok, S.A. Waltner, Z. Wei, H.J. Rathbun, R.M. McMeeking, A.G. Evans, A protocol for characterizing the structural performance of metallic sandwich panels: Application to pyramidal truss cores, Int. J. Solids Struct. 41 (22–23) (2004) 6249–6271.
[51] F. Côté, V.S. Deshpande, N.A. Fleck, A.G. Evans, The compressive and shear responses of corrugated and diamond lattice materials, Int. J. Solids Struct. 43 (20) (2006) 6220–6242.
[52] G.W. Kooistra, V.S. Deshpande, H.N.G. Wadley, Compressive behavior of age hardenable tetrahedral lattice truss structures made from aluminium, Acta Mater. 52 (14) (2004) 4229–4237.
[53] D.T. Queheillalt, H.N.G. Wadley, Cellular metal lattices with hollow trusses, Acta Mater. 53 (2) (2005) 303–313.
[54] D.T. Queheillalt, H.N.G. Wadley, Pyramidal lattice truss structures with hollow trusses, Mater. Sci. Eng. A 397 (1–2) (2005) 132–137.
[55] F. Cote, V.S. Deshpande, N.A. Fleck, A.G. Evans, The out-of-plane compressive behavior of metallic honeycombs, Mater. Sci. Eng. A 380 (1–2) (2004) 272–280.